frontiers in Ecology and Evolution

ORIGINAL RESEARCH
published: 27 May 2020
doi: 10.3389/fevo.2020.00139

Locomotory Adaptations in 3D Humerus Geometry of Xenarthra: Testing for Convergence

*Carmela Serio[1], Pasquale Raia[2] and Carlo Meloro[1]**

[1] Research Centre in Evolutionary Anthropology and Palaeoecology, School of Biological and Environmental Sciences, Liverpool John Moores University, Liverpool, United Kingdom, [2] Dipartimento Di Scienze Della Terra, Dell'Ambiente E Delle Risorse, Università degli Studi Di Napoli Federico II, Naples, Italy

Three-dimensional (3D) models of fossil bones are increasingly available, thus opening a novel frontier in the study of organismal size and shape evolution. We provide an example of how photogrammetry can be combined with Geometric Morphometrics (GMM) techniques to study patterns of morphological convergence in the mammalian group of Xenarthra. Xenarthrans are currently represented by armadillos, sloths, and anteaters. However, this clade shows an incredibly diverse array of species and ecomorphotypes in the fossil record, including gigantic ground sloths and glyptodonts. Since the humerus is a weight-bearing bone in quadrupedal mammals and its morphology correlates with locomotor behavior, it provides an ideal bone to gain insight into adaptations of fossil species. A 3D sample of humerii belonging to extant and fossil Xenarthra allowed us to identify a significant phylogenetic signal and a strong allometric component in the humerus shape. Although no rate shift in the evolution of the humerus shape was recorded for any clade, fossorial and arboreal species humerii did evolve at significantly slower and faster paces, respectively, than the rest of the Xenarthran species. Significant evidence for morphological convergence found among the fossorial species and between the two tree sloth genera explains these patterns. These results suggest that the highly specialized morphologies of digging taxa and tree sloths represent major deviations from the plesiomorphic Xenarthran body plan, evolved several times during the history of the group.

Keywords: photogrammetry, Xenarthra, morphological convergence, geometric morphometrics, RRphylo

OPEN ACCESS

Edited by:
Alexandra Houssaye, UMR7179 Mécanismes Adaptatifs et Evolution (MECADEV), France

Reviewed by:
Leo Botton-Divet, Humboldt University of Berlin, Germany
Sergio Fabián Vizcaíno, Consejo Nacional de Investigaciones Científicas y Técnicas (CONICET), Argentina

****Correspondence:***
Carlo Meloro
C.Meloro@ljmu.ac.uk

Specialty section:
This article was submitted to Paleontology, a section of the journal Frontiers in Ecology and Evolution

Received: *23 December 2019*
Accepted: *24 April 2020*
Published: *27 May 2020*

Citation:
Serio C, Raia P and Meloro C (2020) Locomotory Adaptations in 3D Humerus Geometry of Xenarthra: Testing for Convergence. Front. Ecol. Evol. 8:139. doi: 10.3389/fevo.2020.00139

INTRODUCTION

Species morphology varies in size and shape. These two components can be strongly correlated to each other (Shingleton et al., 2007; Figueirido et al., 2011; Voje et al., 2014; Klingenberg, 2016) and somewhat limited by the existence of evolutionary constraints (Gould, 1989; Brakefield, 2006; Arnold, 2015; Meloro et al., 2015a). In this regard, the vertebrate skeleton has been intensively investigated, because the shape of its components is greatly influenced by body size and by the constraints impinging on specific adaptations linked to body support and other essential organismal functions (e.g., locomotion, feeding). The skeleton also allows sampling ancient diversity that in many clades can greatly overcome variation of extant taxa. In fact, the appreciation of fossil diversity provides strong support for the existence of size-induced shape changes (allometry) across different taxonomic scales and several components of the skeleton (Speed and Arbuckle, 2016).

The combined effects of such size-related shape changes and the evolutionary pressure originated by adaptation might generate patterns of morphological convergence in distantly related clades (Harmon et al., 2005; Mahler et al., 2010; Losos, 2011; Meloro et al., 2015b). Convergence is more likely to take place when adaptation is at the most extreme, and it can be identified in both extant and fossil taxa (i.e., the skulls of marsupial and placental carnivores including sabertooth morphologies, Wroe and Milne, 2007; Goswami et al., 2011).

Extant Xenarthra are currently limited to 31 species falling within the two clades Cingulata (armadillos) and Pilosa (sloths and anteaters; Simpson, 1980; Engelmann, 1985; Springer et al., 2003; Delsuc et al., 2004). Yet, in the past they showed much greater phenotypic and taxonomic diversity, encompassing some 700 species overall, including the gigantic late Pleistocene ground sloths and armadillos (Prothero, 2016).[1] Although recent advances in proteomics and genomics provide new insights into Xenarthra phylogenetic history, their position within Placental mammals is still a matter of controversy (Gibb et al., 2016).

Previous morphological work provided insights into the ecology and behavior of fossil Xenathrans. Most of it was based on the study of body proportions (Bargo et al., 2000; Vizcaíno et al., 2006; Toledo et al., 2017), limb elements (Fariña et al., 2003; Milne et al., 2009; Toledo et al., 2015; Mielke et al., 2018), and the skull (Vizcaíno et al., 1998; De Iuliis et al., 2001; Bargo and Vizcaíno, 2008; Billet et al., 2011). For a full revision, see Bargo (2003); Vizcaíno et al. (2008), Amson and Nyakatura (2017), and Bargo and Nyakatura (2018).

Thanks to 3D modeling, it is currently possible to build precise replicas of fossil bones and investigate their size and shape variation with better accuracy than ever before. Applying such 3D modeling on Xenarthran limb elements is particularly welcome, given the great diversity of size and lifestyle the group experienced in its recent past (Amson and Nyakatura, 2017).

Here, we combine multiple methods for the 3D analysis and interpretation of Xenarthra humerus shape variation within a phylogenetic comparative framework. The humerus is a load-bearing postcranial element in quadrupedal mammals (Bertram and Biewener, 1992) and correlates quite strongly with body mass, locomotory, and habitat adaptations (Gingerich, 1990; Egi, 2001; Elton, 2002; Polly, 2007; Walmsley et al., 2012; Meloro et al., 2013; Elton et al., 2016; Botton-Divet et al., 2017). In Xenarthrans, the broad locomotory diversity well correlates with humerus functional morphology (Fariña and Vizcaíno, 1997; Toledo et al., 2012; de Oliveira and Santos, 2018).

We take advantage of the newly developed photogrammetry technique (Falkingham, 2012) to build a dataset of 51 Xenarthran humerus 3D models belonging to 29 species (16 extant plus 13 extinct). The advantage of photogrammetry is that it minimizes specimen handling (which is convenient for their fragile status) and allows a relatively quick data collection based on museum specimens (taking pictures for photogrammetry models might take between 5 and 10 min; Giacomini et al., 2019). On the other side, software post-processing time can still be quite long, although the development of professional software (e.g., Agisoft) and novel open access sources are making the process increasingly quicker.[2] There has been a lot of research focusing on the adequacy and the accuracy of photogrammetry method for GMM analyses (see Giacomini et al., 2019, for a recent overview). Particularly for long bones, Fau et al. (2016) demonstrated that photogrammetry provides a good level of accuracy compared to other laser scanners (e.g., structured light Artec laser or Breukmann) on relatively medium-sized vertebrate long bones.

We explored Xenarthran humerus 3D morphology using GMM within a comparative framework. This technique is now well established with a long record of research applications also on fossil mammals (Adams et al., 2004, 2013). The use of homologous points (landmarks) facilitates a comparison between species belonging to the same clade and additionally provides a powerful tool for separating and visualizing size and shape variations. GMM application to the study of Xenarthran functional morphology includes works from Monteiro and Abe (1999) focusing on the scapula or Milne et al. (2009, 2012) on humerus and femur shape.

Interestingly, the implementation of the comparative methods into GMM datasets is a relatively more recent phenomenon. Comparative methods were first introduced by Felsenstein in his seminal paper on the independent contrasts (Felsenstein, 1985). This method explores the assumption that interspecific data are not independent, since species might share a different degree of common ancestry in any macroevolutionary dataset. The effect of shared inheritance can be assessed by estimating the "phylogenetic signal" in the data. When fossil species are concerned, two major limitations occur: fossil phylogenies are morphology based, so that testing morphological hypotheses using these trees might generate a circular argument (in the majority of cases fossil dataset might exhibit higher phylogenetic signal); fossil phylogenies are generally incomplete with taxonomic confirmation generally scattered between different publications. In spite of this, early attempts demonstrated that fossil phylogenies can be incorporated to test macroevolutionary hypotheses, and their inclusion provides stronger statistical power (for early examples see: Finarelli and Flynn, 2006; Meloro et al., 2008). We provided on several occasions examples on how comparative methods can be implemented in macroevolutionary studies incorporating fossils and GMM (Meloro and Raia, 2010; Raia et al., 2010; Meloro and Slater, 2012; Piras et al., 2012). More recently, the development of new R packages (including geomorph Adams et al., 2019; and *RRphylo* Raia et al., 2020) allows to detect evolutionary rates with a high degree of accuracy (in spite of phylogenetic fossil uncertainty, e.g., Smaers et al., 2016; Castiglione et al., 2018).

We take advantage of the most recently published phylogenies for fossil sloths and armadillos in order to test hypotheses about the influence of size and locomotor behavior on humerus shape and rate of its morphological change in Xenarthra. Since behavioral and morphological convergence has been proposed for extant sloths, as well as fossil *Megatherium* and extant armadillos (Nyakatura, 2012; Billet et al., 2015), we explicitly tested convergence in humerus morphology using a

[1] https://paleobiodb.org/#/

[2] https://peterfalkingham.com/tag/photogrammetry/

novel approach that can well be applied to multivariate shape data and phylogenies inclusive of extant and fossil species (Castiglione et al., 2019).

MATERIALS AND METHODS

Studied Specimens

We built 3D models of Xenarthra humerii belonging to 29 species housed at the following museum institutions: the Natural History Museum (NHLM, London) and the Muséum National d'Histoire Naturelle (MNHN, Paris, see **Supplementary Table S1** for details).

For each specimen, we took about 200 photos based on dorsal, ventral, and lateral views using a dark background and a standard digital SLR (Nikon D5300, lens 18–140 mm). Most of the pictures were taken with the 55 mm lens setting on a fixed focus (see Giacomini et al., 2019). The software Agisoft Metashape was then employed to build 3D models, while MeshLab software (v1.3.3, 2014) was used for scaling them. The scaling was based on one single measurement (generally the maximum bone length), as recommended by Falkingham (2012). Sensitivity analyses testing relative bone proportion were performed on selected specimens of similar-sized mammalian humerii, generally providing a difference smaller than 5% when comparing measurements taken with digital caliper and those with the MeshLab software (v1.3.3, 2014).

Landmarking

The software Landmark (v. 3.0) was employed to identify on each specimen 28 landmarks (**Figure 1**). The landmarks were designed to cover main anatomical regions of the Xenarthran humerus including proximal and distal epiphyses as possible. The Landmark descriptions are in **Table 1** following anatomical nomenclature (**Figure 1**). Most of the landmarks were type 2, since humerus epiphyses do not allow to identify type 1 points. However, these were previously evaluated in Milne et al. (2009), which we followed as a baseline for our configuration (see **Table 1** and **Figure 1**). Landmarking was performed twice on a subsample of 20 specimens to detect the level of error in size and shape using Procrustes ANOVA, which in all cases turned out to be non-significant explaining less than 5% of inter-individual variation.

GMM and Comparative Methods

The 3D landmarked coordinates of the scaled models were subject to GPA (Generalized Procrustes Analysis, Rohlf and Slice, 1990). This technique removes the non-shape information related to size, position, and orientation of the specimens. GPA returns a new set of coordinates subsequently subjected to Principal Component Analysis (PCA, Rohlf and Slice, 1990). PCA decomposes the shape variation into orthogonal axes of maximum variation named PCs (Principal Components). PC vectors are used as variables in subsequent analyses. Species mean shapes were calculated before performing analyses so that our shape data represented inter-specific variation only. Humerus size was quantified using the natural logarithm (Ln) of the centroid size (=the square root of the sum of the squared distances from each landmark to the centroid of each configuration).

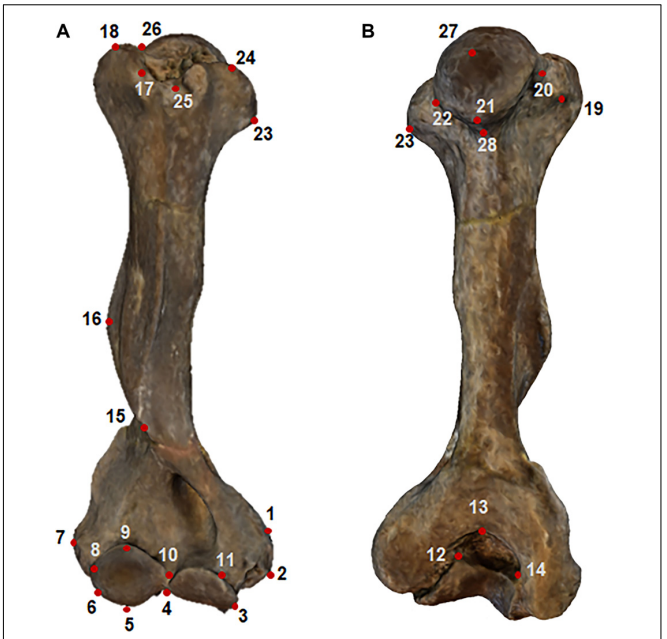

FIGURE 1 | Humerus model of Thallassocnus littoralis built using the photogrammetry method. Dots represent digitised anatomical landmarks. **(A)** frontal view, **(B)** posterior view.

We assembled two different phylogenetic trees. The first was based on molecular data following Presslee et al. (2019) and Raia et al. (2013; **Supplementary Data S1**). The second tree was based on purely morphological evidence and assembled on a backbone published in Delsuc et al. (2019); Varela et al. (2019), Boscaini et al. (2019); Fernicola et al. (2017), Herrera et al. (2017), and Gaudin and Wible (2006; **Supplementary Data S2**). We decided to use two different phylogenies because molecular vs. morphological trees may be conflicting (Cohen, 2018). For the phylogenetic position of species for both trees and references see **Supplementary Table S2**. The phylogenetic trees were calibrated by using the *scaleTree* function in the *RRphylo* package (Raia et al., 2020, species last appearance and internal node ages used for calibration are in **Supplementary Table S2**).

By using *plotGMPhyloMorphoSpace* function in the geomorph package (Adams et al., 2019), the trees were mapped into PCA in order to generate a phylomorphospace. Phylogenetic signals were quantified by using the K (for size) and the K_{multiv} (for shape) statistic (Adams, 2014).

Phylogenetic Generalized Least Squares (PGLS) regression was employed assuming Brownian motion as the mode of evolution to test for macroevolutionary allometry and differences among locomotory categories. We partitioned species into discrete stance categories as proposed by Amson et al. (2017) based on the main lifestyle of extant taxa. Tree sloths were considered as fully "arboreal." The anteaters, capable of both climbing and having a unique digging style, were classified as "intermediate" (Hildebrand, 1985; Kley and Kearney, 2007),

TABLE 1 | Landmark descriptions.

Landmark	Anatomical definitions
1	Point of maximum curvature of the medial epicondyle
2	Point of minimum curvature of the medial epicondyle
3	Trochlea bottom point
4	Point of maximum curvature in the trochlea, lower section
5	Most distal portion of the capitulum, lower section
6	Most proximal portion of the capitulum, lower section
7	Point of maximum projection of the lateral epicondyle
8	Most proximal portion of the capitulum, upper section
9	Most distal portion of the capitulum, upper section
10	Point of maximum curvature of trochlea, upper section
11	Highest point on the interior edge of the trochlea
12	Lateral point (sx) of olecranon fossa
13	Deepest point of olecranon fossa
14	Lateral point (dx) of olecranon fossa
15	Point of intersection between epicondylar ridge and deltoid crest
16	Point of maximum lateral projection of the deltoid crest
17	Proximal limit of the greater tubercle
18	Highest proximal point of the greater tubercle
19	Distal limit of the greater tubercle
20	Point of intersection between lesser tubercle and humeral head
21	Most proximal limit of the humerus head epiphyseal surface
22	Edge of the lesser tubercle intersecting the humerus head
23	Proximal limit of the lesser tubercle
24	Distal limit of the lesser tubercle
25	Bicipital sulcus
26	Point of intersection between greater tubercle and humeral head
27	Highest projection on the humerus head articular surface
28	Point of intersection between lesser tubercle and humeral neck

whereas armadillos were divided into fully "terrestrial" and "fossorial." For fossil species, we carried out an extensive revision of the literature (see **Supplementary Table S3**). Extant members of Cingulata are specialized diggers as inferred by their limb morphology (Vizcaíno and Milne, 2002; Milne et al., 2009; Marshall, 2018; Mielke et al., 2018). Other specialized diggers can be found also among Pilosa. *Glossotherium robustum* was demonstrated to be a specialized digger (Bargo et al., 2000; Vizcaíno et al., 2001; de Oliveira and Santos, 2018). On the contrary, other ground sloths were best adapted to a terrestrial lifestyle (Bargo et al., 2000; Vizcaíno et al., 2001; de Oliveira and Santos, 2018). Extant sloths (*Bradypus* and *Choloepus*) are known as tree sloths for their strictly arboreal lifestyle (Montgomery, 1985; Chiarello, 2008; Toledo et al., 2012), as well as the anteaters (White, 2010), but the latter are capable of above branch locomotion (Nyakatura, 2011). Locomotor categories were equally employed to test for convergence.

We assessed the rate of humerus size and shape evolution by using the *RRphylo* function (Castiglione et al., 2018). *RRphylo* returns a vector of evolutionary rates for all branches in the tree and a vector (or a matrix if the phenotype is multivariate, i.e., with the shape data) of ancestral states estimated for each node. We applied *RRphylo* on both size (log-transformed) and shape (as PC scores and by using size as covariate).

To search for possible shifts in the evolutionary rates between clades or locomotory categories we used the function *search.shift* (Castiglione et al., 2018). First, we applied *search.shift* on shape and size under the "clade" condition. In this case, the function compares the average absolute evolutionary rate of a specific clade with the rest of the tree. The significance level is assessed by randomizations. Then, we applied *search.shift* on shape and size under the "sparse" condition to test for differences in evolutionary rates among locomotor categories. Under this condition, the function tests if species having the same state evolve differently from the others.

Eventually, we applied the new function *search.conv* (Castiglione et al., 2019) to test for morphological convergence. This function tests morphological convergence by assessing the angle between phenotypic vectors (vectors of PC scores) between species and comparing this angle to a random expectation. Given two phenotypic vectors (here PC scores), the cosine of angle θ between them represents the correlation coefficient (Zelditch et al., 2012). Under the Brownian Motion, θ is expected to be proportionally related to phylogenetic distance. Yet, convergence violates this assumption. The new method *search.conv,* calculates the θ angles between entire clades ("automatic") or species under the same state ("state"). It tests whether the mean θ between the species evolving under a specific state or belonging to a single clade is smaller than expected by chance, and whether θ divided by the mean phylogenetic distance among convergent tips is smaller than expected. We applied *search.conv* to test for morphological convergence between fully arboreal sloths and the intermediate anteaters, and species evolving under fossorial lifestyles. Then, we tested convergence between the two tree sloths: *Bradypus* and *Choloepus*.

To test the robustness of our results to phylogenetic uncertainty and sampling effects, we applied the new implemented function *overfitRR* (Serio et al., 2019; Melchionna et al., 2020) in the *RRphylo* package (Raia et al., 2020). Under this function, the original tree is trimmed of a predetermined number of species (here 5%) and the position of tips is changed randomly by up to two nodes away from its original placement. For instance, a simple phylogenetic tree [(A, B), C], would be changed in [(C, B), A] or [(A, C), B] tree topology. In addition, the function changes the node age, randomly, within a range between the age of the focal node immediate ancestor node and the age of its older daughter node. We ran *overfitRR* with 100 iterations. At each iteration, the function swapped 5% of the tree size of tips and changed in age 5% of the tree size of tree nodes, then used a new phylogenetic tree to perform *search.conv* to either confirm or reject any instance of significant morphological convergence. All the analyses were performed both with the molecular and the morphological phylogenies.

RESULTS

Geometric Morphometric Results

GMM returned 28 PCs (**Supplementary Table S4**), of which the first 13 explained up to 95.80% of the shape variation. More in detail, PC1 and PC2 explained 53.58% and 15.72%, respectively,

and they show a degree of separation in humerus shape between Cingulata and Folivora, while Vermilingua clade overlap with the latter (**Figure 2**).

Deformations described by PC1 are related to the relative elongation of the humerus. Arboreal species occupy positive scores of PC1 and are characterized by a relatively longer and slender humerus morphology. Both proximal and distal epiphyses are reduced. This configuration is typical of the suspensory tree sloths (genera *Bradypus* and *Choloepus*). On the contrary, PC1 negative scores describe short and stocky humerus shape. The head and both the greater and lesser tuberosities are more expanded, as well as the trochlea, capitulum, and epicondyles (**Figure 2**).

Changes along PC2 axis described differences among Xenarthra clades. Folivora and Vermilingua occupy positive PC2 scores. In these clades, the humerus head is slender, the curvature between the deltoid crest and the distal part is wider and developed backward. On the negative scores of PC2, Cingulata shows distinct humerus head components with the distal part longer and slender (**Figure 2**).

Comparative Methods

When applying the molecular tree, the phylogenetic signal for both shape and size was statistically significant. The observed K (size) and K_{multiv} (shape) are 0.997 and 0.453 (p value = 0.001), respectively. Very similar results were obtained when the morphological tree was used (K size = 0.939; p value = 0.001, K_{multiv} shape = 0.497, p value = 0.001).

Differences in shape were explained by differences in size, as resulted by using Procrustes ANOVA without (**Table 2A**) and with the addition of the phylogenetic effect of the morphological tree (**Table 2C**). The allometric effect remained significant in Folivora and Cingulata when the phylogenetic relationship was accounted for (**Table 3** and **Figure 3**). Procrustes ANOVA showed a significant impact of locomotor categories on shape, either without considering phylogenetic effects or by using the molecular tree (**Table 2**). However, locomotion had no impact on humerus size variation (**Table 2**).

By applying *search.shift* to the humerus size, we found a significant increase in evolutionary rates in the clade, including Mylodontidae and *Choloepus* (average rate difference = 0.080, p = 0.001; **Figure 4A**), and a significant decrease in the clade, including *Panoctus*, *Doedicurus*, *Neosclerocalyptus*, and *Hoplophorus* (average rate difference = −0.025, p = 0.006; **Figure 4A**). This same negative shift applied when the morphological tree was considered (average rate difference = −0.020, $p < 0.001$; **Figure 4B**), whereas a positive rate shift was found for the clade including Euphractinae and

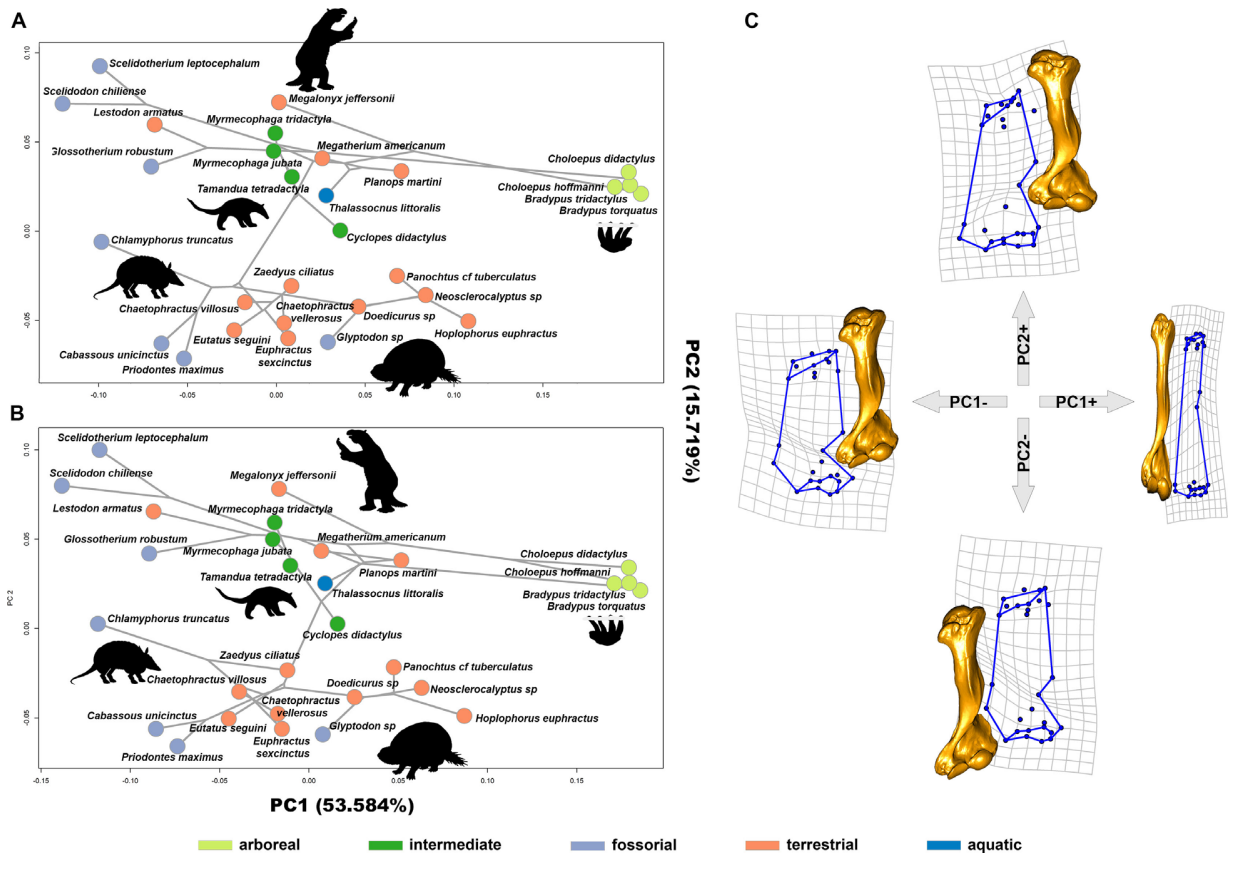

FIGURE 2 | Phylomorphospaces of PC1 vs. PC2 mapping molecular **(A)** and morphological tree **(B)**. Gray lines connect species with their reconstructed ancestral node. **(C)** Deformation grids and warping model (by using as reference *T. littoralis*).

TABLE 2 | Xenarthra summary statistics for different Procrustes ANOVA models without (A) and with (B, C) accounting for the phylogenetic effect.

Model	SS	MS	R^2	F	p values
(A) Proc ANOVA without phylogeny					
Shape∼size	0.069	0.069	0.160	5.156	**0.008**
Shape∼loc	0.102	0.026	0.238	1.870	**0.044**
Size∼loc	1.894	0.473	0.077	0.503	0.736
(B) Proc ANOVA with molecular tree					
Shape∼size + phy	0.001	0.001	0.068	1.960	0.097
Shape∼loc + phy	0.006	0.001	0.269	2.210	**0.016**
Size∼loc + phy	0.109	0.027	0.196	1.464	0.256
(C) Proc ANOVA with morphological tree					
Shape∼size + phy	0.002	0.002	0.104	3.146	**0.022**
Shape∼loc + phy	0.002	0.001	0.147	1.034	0.408
Size∼loc + phy	0.022	0.005	0.042	0.264	0.881

SS, the Sums of Squares; MS, Mean squares; R^2, the coefficient of determination for each model term; F, The F values for each model term; p values, probability computed for each model, significance (<0.05) is highlighted in bold; loc = locomotion.

TABLE 3 | Folivora and Cingulata summary statistics for different Procrustes ANOVA models without (A) and with (B, C) accounting for phylogenetic effect.

Group	Model	SS	MS	R^2	p values
(A) Proc ANOVA without phylogeny					
Folivora	shape∼size	0.125	0.125	0.562	**0.003**
Cingulata		0.037	0.037	0.345	**0.003**
(B) Proc ANOVA with molecular tree					
Folivora	shape∼size + phy	0.004	0.001	0.258	**0.008**
Cingulata		0.000	0.000	0.091	0.333
(C) Proc ANOVA with morphological tree					
Folivora	shape∼size + phy	0.004	0.004	0.439	**0.001**
Cingulata		0.002	0.002	0.342	**0.024**

SS, the Sums of Squares; MS, Mean squares; R^2, the coefficient of determination for each model term; F, The F values for each model term; p values, probability computed for each model, significance (<0.05) is highlighted in bold; loc = locomotion.

Chlamyphorus (average rate difference = 0.047, $p < 0.001$; **Figure 4B**) by using this tree. We did not find significant shifts in the rate of humerus shape evolution with either tree.

By testing for rate shifts in humerus size per locomotory state, we found a positive and significant difference in rates pertaining to strictly arboreal species (tree sloths) by using molecular trees (rate difference = 0.123, p value = 0.001, **Table 4**). Similarly, tree sloths showed significantly higher rates of shape evolution as compared to the rest of the taxa (rate difference = 11.259, p value <0.001, **Table 4**). With this same molecular tree, fossorial species had slower rates of humerus shape evolution as compared to the species falling in different locomotory states (rate difference = −2.040, $p = 0.002$, **Table 4**). When applying the morphological tree, these differences were less apparent although fossorial species still showed slower, and arboreal species higher rates as compared to the rest of the taxa, either by analyzing humerus size or shape (**Table 4**).

By using *search.conv*, we tested the convergence in humerus shape between species living on tree branches although ascribed to different categories (intermediate and arboreal). *search.conv* returned a non-significant angle of 98.253° (p value = 0.867) between the species under the two states, the same applied when the angle was tested per unit time (p value = 0.099; **Table 5A**). A strong evidence for convergence appears within the strictly arboreal species, that is the *Bradypus* and *Choloepus* clades (θ_{real} = 0.235, $p\theta_{real}$ = 0.010; ($\theta_{real+\theta ace}$)/time = 0.383, p($\theta_{real+\theta ace}$)/time = 0.001; **Table 5B** and **Figures 5B,D**). Morphological convergence was additionally found for species evolving in the "fossorial" category (mean angle among fossorial species = 68.148°; p angle state = 0.002, **Table 5A** and **Figure 5C**). This notion is confirmed when the time distance between species is accounted for (θ_{time} = 0.786, $p\theta_{time}$ = 0.001, **Table 5A**).

overfitRR returned 0% of significant simulations when convergence between the arboreal and intermediate states is tested for both phylogenies. This is in agreement with *search.conv* results.

For the issue of convergence between *Bradypus* and *Choloepus* *overfitRR* returned 100% (for both θ_{real} and $\theta_{real+\theta ace}$)/time) instances of significance by using molecular tree. When the same analysis is performed by using morphological tree, *overfitRR* returned 71% for θ_{real} and 74% for $\theta_{real+\theta ace}$)/time instance of significant convergence.

For the issue of convergence between fossorial species, *overfitRR* returned 100% ($p.\theta_{state}$) and 99% ($p.\theta_{time}$) of significant p values when molecular tree is used. The same figures for the morphological tree were 100% ($p.\theta_{state}$) and 98% ($p.\theta_{time}$).

DISCUSSION

The taxonomic and phenotypic diversity of extant Xenarthrans represents only a small fraction of their past variations. Perhaps unsurprisingly, giant extinct glyptodonts (*Doedicurus*, *Glyptodon*, and their allies) experienced a shift toward a slow rate of size evolution, in keeping with their uniformly large body size. This stands true irrespective of whether molecular or morphological trees are used. In contrast, a significant positive shift in the rate of humerus size evolution appears in Euphractinae plus *Chlamyrophus* by using the morphological tree only, with *Eutatus* placed outside the clade of Glyptodontinae plus Euphractinae (**Figure 4B**). This probably related with a decrease in size of Euphractinae plus *Chlamyrophus* in contrast with the plesiomorphic condition of *Eutatus*, whose estimated body size is supposed to range between 36.8 and 71.7 kg (Vizcaíno and Bargo, 2003). On the contrary, extant Euphractine plus *Chlamyrophus* are only 2 kg in body size on average.

We found no significant instance of shape evolutionary shifts pertaining to the Xenarthran trees, meaning that major shape differences were channelled through phylogeny as further supported by GMM results. Phylomorphospace showed a neat separation between the two clades Cingulata and Pilosa along PC2 (**Figure 2**).

However, the humerus changed significantly relative to locomotory styles. The rate of shape evolution in fossorial

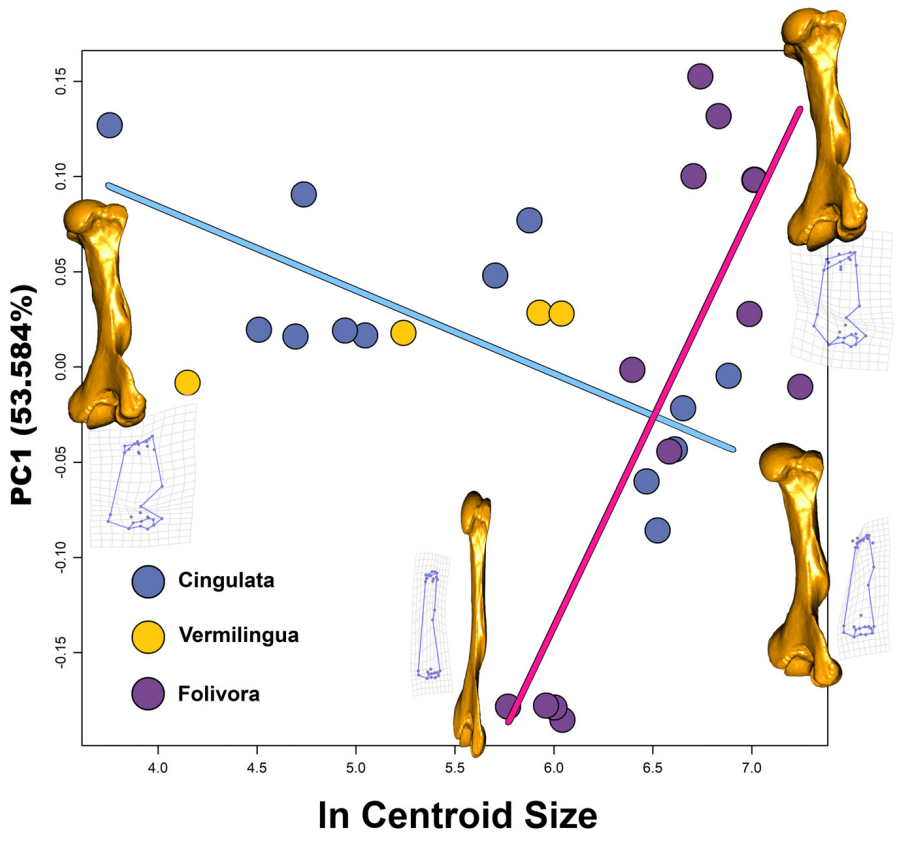

FIGURE 3 | Ln Centroid Size vs. PC1 scatter plot. Regression for Cingulata is represented by the light blue line. Regression for Folivora is represented by the pink line. At the extreme of PC1 for both groups are present the grids showing shape deformations and warping models (by using as reference *T. littoralis*).

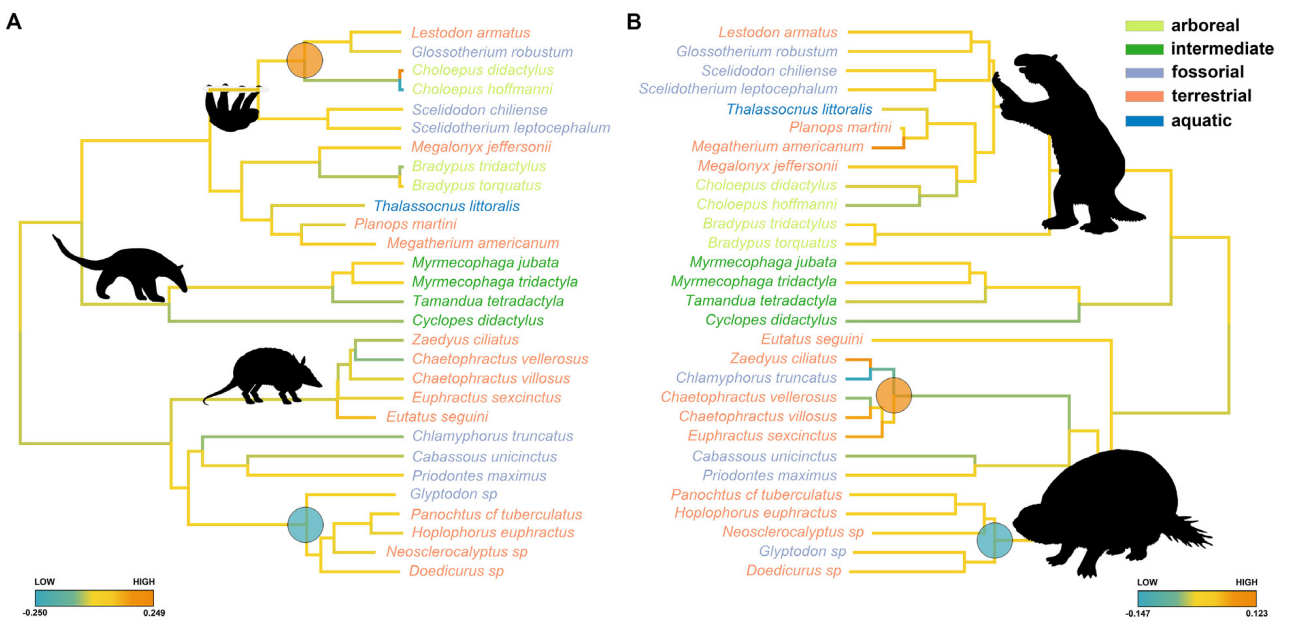

FIGURE 4 | Evolutionary rates (color coded) for the Xenarthra humerus size along the molecular **(A)** and morphological **(B)** tree. Species names are coded according to locomotor categories. Large dots at nodes represent clade shifting (blue = low, orange = high).

TABLE 4 | *search.shift* results for size showing shift in evolutionary rate.

	Molecular tree				Morphological tree			
	Size		Shape		Size		Shape	
	Rate difference	*p* values	Rate difference	*p* values	Rate difference	*p* values	Rate difference	*p* values
arboreal – aquatic	0.134	**0.002**	11.99	**<0.001**	−0.001	0.372	−1.457	0.158
fossorial – aquatic	0.004	0.367	0.045	0.311	0.017	0.636	−2.604	**0.049**
intermediate – aquatic	0.017	0.543	0.725	0.476	0.003	0.403	−3.021	**0.041**
terrestrial – aquatic	0.014	0.464	1.159	0.469	0.017	0.595	−1.107	0.179
fossorial – arboreal	−0.129	**0.003**	−11.945	**0.001**	0.018	0.777	−1.148	0.166
intermediate – arboreal	−0.117	**0.005**	−11.265	**0.001**	0.004	0.528	−1.564	0.127
terrestrial – arboreal	−0.12	**0.004**	−10.832	**0.001**	0.018	0.811	0.349	0.601
intermediate – fossorial	0.012	0.673	0.68	0.604	−0.015	0.247	−0.416	0.421
terrestrial – fossorial	0.009	0.565	1.114	0.702	0.000	0.481	1.497	0.969
terrestrial – intermediate	−0.003	0.373	0.433	0.501	0.015	0.762	1.913	**0.015**
terrestrial	−0.026	0.162	−2.04	0.081	0.009	0.758	1.151	0.957
fossorial	−0.031	0.086	−2.952	**0.008**	0.007	0.691	−1.136	0.054
intermediate	−0.013	0.473	−1.808	0.286	−0.011	0.319	−1.482	**0.045**
aquatic	−0.029	0.425	−2.366	0.188	−0.015	0.251	0.332	0.742
arboreal	0.123	**0.001**	11.259	**<0.001**	−0.013	0.492	1.805	0.918

Rate difference is computed as the average rate for all species evolving under the same state minus the average for each other state (for group comparison) or the rest of the tree (for the single state). p values is assessed by means of randomization.

Xenarthrans is significantly smaller than in other species. Such fossorial habitus characterizes most Cingulata and is possibly plesiomorphic to the group (Vizcaíno and Milne, 2002; Milne et al., 2009; Marshall, 2018), although it is surprisingly present among giant ground sloths like *Glossotherium* (Bargo et al., 2000; Vizcaíno et al., 2001; de Oliveira and Santos, 2018).

Conversely, arboreal species evolved at faster rates than in any other Xenarthra. Tree sloths were noted for their highly derived and convergent morphologies, canalizing change from a plesiomorphic, fossorial condition (Nyakatura, 2011; Nyakatura and Fischer, 2011), although it must be emphasized that scansorial species (which were not included in the analyses here) were present since the Miocene (Pujos et al., 2012; Toledo et al., 2017).

Overall, our results suggest that the acquisition of arboreal and fossorial lifestyles are loaded with great functional demands, leading to constrained, little variable morphologies (fossorial) or to significant changes in shape toward a particular configuration (from the ancestral conditions) to match a demanding lifestyle (arboreal sloths). These challenging adaptations present ideal cases to test convergence. We provided this test for both fossorial species and tree sloths, separately, and confirmed they do represent significant instances of morphological convergence (**Figure 5**). The same applies if phylogenetic uncertainty is accounted for. The results further support the observation that phylogenetic signal in humerus shape is as much high as for humerus size (Vizcaíno et al., 1999; Vizcaíno and Bargo, 2003), but also suggest that tree-living is the room for morphological change among Xenarthran taxa.

Limb proportions in fossil *Eutatus* were similar to extant Euphractine (Vizcaíno and Bargo, 2003). These species present limbs specialized in building borrows rather than in gathering food (Vizcaíno and Bargo, 2003). Thus, the high size evolutionary rates can be related with more robust humerii specialized for digging. It was demonstrated that Miocene glyptodonts weighed about 100 kg, but Pleistocene species may have weighed up to 1 ton (Vizcaíno et al., 2010; Milne et al., 2012). Our results indicate that the lowest evolutionary rate in humerus size occurs in *Panoctus*, *Doedicurus*, *Neosclerocalyptus*, and *Hoplophorus* suggesting humerus size in these taxa was linked to their large but uniform body size.

Xenarthra originated in South America about 62.5 million years ago (Presslee et al., 2019). During the Great Biotic Interchange in late Pliocene (Marshall et al., 1979; Webb, 2006)

TABLE 5 | Convergence results.

(A) *search.conv* results under "state" condition

state	θ_{state}	$p.\theta_{state}$	θ_{time}	$p.\theta_{time}$
Arboreal – intermediate	98.253	0.867	0.945	0.099
Fossorial	68.148	**0.002**	0.786	**0.001**

(B) *search.conv* results under "automatic" condition

node	θ_{real}	$p\ \theta_{real}$	$(\theta_{real+\theta ace})$/time	$p(\theta_{real+\theta ace})$/time
Bradypus – Choloepus	0.235	**0.01**	0.383	**0.001**

(A) Results as returned by search.conv. θ_{state}: mean angle between species within a within a single state; $p.\theta_{state}$: p value computed for θ_{state}. (B) Results as returned by search.conv for clade subtending Bradypus and Choloepus.θ_{real}: the mean angle between Bradypus and Choloepus divided by the time distance; p θ_{real}: the p-value computed for θ_{real}; $(\theta_{real+\theta ace})$/time: the mean theta angle between Bradypus and Choloepus plus the angle between aces, divided by the time distance; $p(\theta_{real+\theta ace})$/time: the p-value computed for $(\theta_{real+\theta ace})$/time. Significant p values (<0.05) are highlighted in bold.

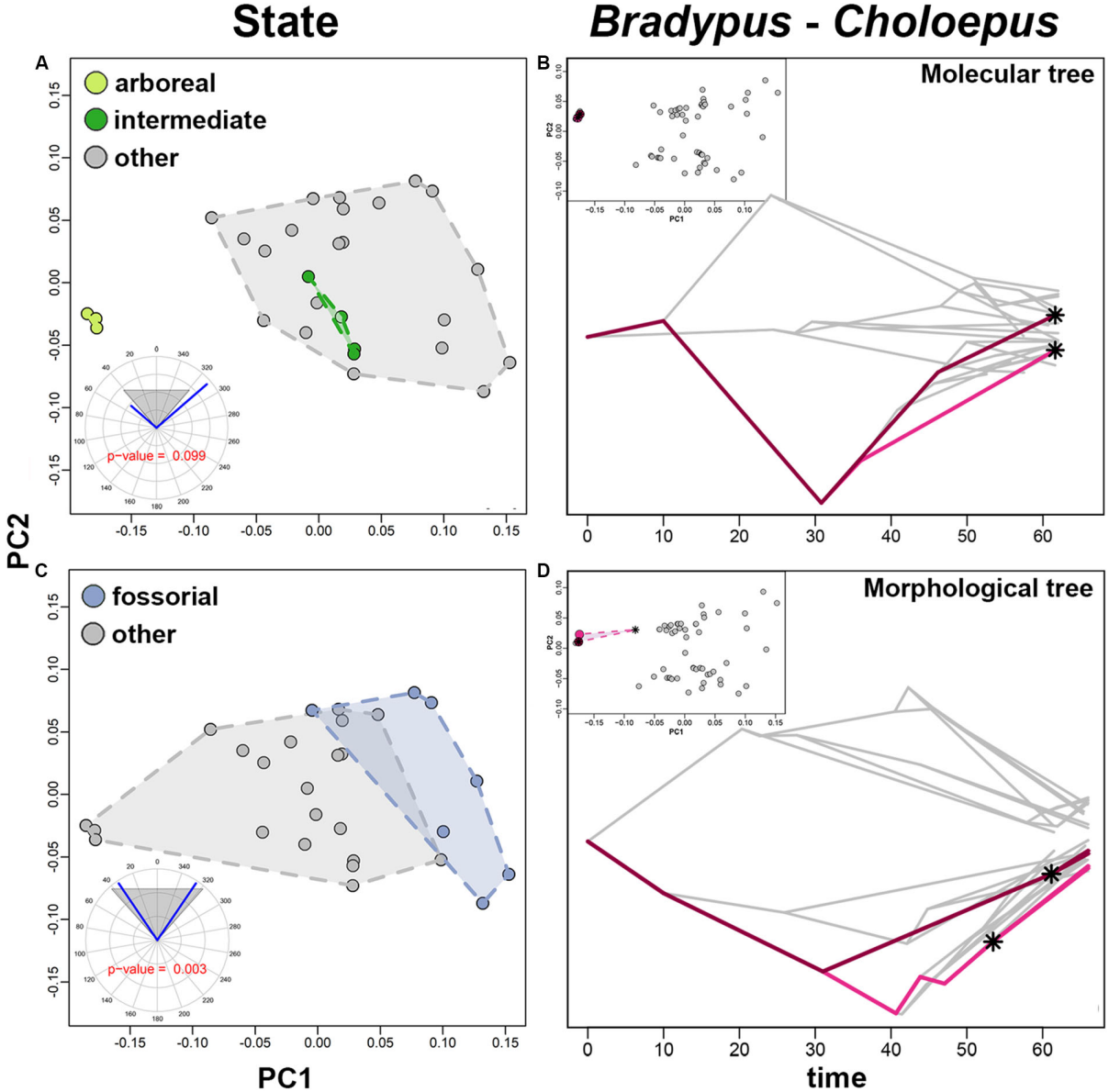

FIGURE 5 | (A,C) PC1 vs. PC2 scatter plot. Convex hulls are colored according to different states. Circular plots represent the mean angle between states, the gray area is the random angle range. **(B,D)** Traitgram plot with colored branched representing convergent clade. PC1 vs. PC2 scatter plot are produced, convergent clades are color coded. In both, traitgram and PC1 vs. PC2 scatter plot asterisks represent the ancestral phenotypes of the individual clades.

several species migrated to the North (Bocherens et al., 2017). Studies of fossil species have demonstrated that none of the known fossil sloths had arboreal lifestyle (White, 2010; Nyakatura, 2011). The last common ancestor of sloths probably was terrestrial or semi-arboreal (White, 2010; Nyakatura, 2012). Indeed, fossil sloths appear morphologically closer to extant Vermilingua (i.e., *Tamandua* and *Myrmecophaga,* herein classified as "intermediate") rather than to extant tree sloths (Toledo et al., 2012). We did not find instance of convergence among intermediate and arboreal species (**Figure 5**). This supports the idea that modern tree sloths acquired the suspensory habitus secondarily, which explains their higher shape evolutionary rates as compared to the humerii of species ascribed to different locomotor categories. Similarly, the long branch separating the extant tree sloth genera (Presslee et al., 2019) are suggestive of secondary adaptation. Extant sloths present a forelimb-dominated locomotion. *Bradypus* moves up to 10 m only using his forelimbs, and *Choloepus* hind limbs lost their primarily propulsive elements (Mendel, 1985; Nyakatura et al., 2010).

Similarly, since digging kinematics is one of the most demanding behaviors the mammalian skeleton could be designed for Sansalone et al. (2019), the pervasive call for convergence

to a functionally optimal design linked to digging was expected (Sansalone et al., 2020).

One obvious caveat we urge to consider is that, although nearly one-half of the species we considered in our tree are extinct, the history of Xenarthra cautions against giving too much faith to phylogenetic analyses using a tree devoid or otherwise scarce in terms of fossil species representation. The inclusion of fossil phenotypes is, and must carefully be, considered in trait evolution inference, especially when major patterns such as morphological convergence are sought after.

DATA AVAILABILITY STATEMENT

The datasets for this study are included in the **Supplementary Material**.

AUTHOR CONTRIBUTIONS

CS, PR, and CM conceived the project. CS and CM prepared samples and conducted the data analyses. All the authors discussed the results and wrote the manuscript.

FUNDING

CS was supported for this study by LJMU Ph.D. studentship fund.

ACKNOWLEDGMENTS

The authors are grateful to Alessandro Marques de Oliveira for sharing 3D models of Xenarthra humerii. More in details we acknowledge museum curators that hosted previous data collection in London (NHM, Roberto Portela Miguez, Pip Brewer), and Paris (MNHN, Guillaume Billet). Silvia Castiglione helped us to prepare an updated version of *overfitRR* explicitly tailored to work with small trees. The editor AH and the two reviewers equally helped us to improve this presented manuscript.

SUPPLEMENTARY MATERIAL

The Supplementary Material for this article can be found online at: https://www.frontiersin.org/articles/10.3389/fevo.2020.00139/full#supplementary-material

REFERENCES

Adams, D. C. (2014). Quantifying and comparing phylogenetic evolutionary rates for shape and other high-dimensional phenotypic data. *Syst. Biol.* 63, 166–177. doi: 10.1093/sysbio/syt105

Adams, D. C., Collyer, M. L., and Kaliontzopoulou, A. (2019). *Geomorph: Software for Geometric Morphometric Analyses. R Package Version* 3.1.0. Available at: https://cran.r-project.org/package=geomorph (accessed September 3, 2019).

Adams, D. C., Rohlf, F. J., and Slice, D. E. (2004). Geometric morphometrics: ten years of progress following the "revolution". *Ital. J. Zool.* 71, 5–16. doi: 10.1080/11250000409356545

Adams, D. C., Rohlf, F. J., and Slice, D. E. (2013). A field comes of age: geometric morphometrics in the 21st century. *Hystrix* 24, 7–14. doi: 10.4404/hystrix-24.1-6283

Amson, E., Arnold, P., van Heteren, A. H., Canoville, A., and Nyakatura, J. A. (2017). Trabecular architecture in the forelimb epiphyses of extant xenarthrans (Mammalia). *Front. Zool.* 1:52. doi: 10.1186/s12983-017-0241-x

Amson, E., and Nyakatura, J. A. (2017). The postcranial musculoskeletal system of xenarthrans: insights from over two centuries of research and future directions. *J. Mamm. Evol.* 25, 459–484. doi: 10.1007/s10914-017-9408-7

Arnold, S. J. (2015). Constraints on phenotypic evolution. *Am. Nat.* 140, S85–S107. doi: 10.1086/285398

Bargo, M. S. (2003). Biomechanics and palaeobiology of the Xenarthra: the state of the art. *Sencken Biol.* 1, 41–50.

Bargo, M. S., and Nyakatura, J. A. (2018). Morphology and evolution of the xenarthra: an introduction. *J. Mamm. Evol.* 4, 445–447. doi: 10.1007/s10914-017-9419-4

Bargo, M. S., and Vizcaíno, S. F. (2008). Paleobiology of pleistocene ground sloths (Xenarthra, Tardigrada): biomechanics, morphogeometry and ecomorphology applied to the masticatory apparatus. *Ameghiniana* 1, 175–196.

Bargo, M. S., Vizcaíno, S. F., Archuby, F. M., and Blanco, R. E. (2000). Limb bone proportions, strength and digging in some Lujanian (Late Pleistocene-Early Holocene) mylodontid ground sloths (Mammalia, Xenarthra). *J. Vertebr. Paleontol.* 3, 601–610.

Bertram, J. E. A., and Biewener, A. A. (1992). Allometry and curvature in the long bones of quadrupedal mammals. *J. Zool.* 226, 455–467. doi: 10.1111/j.1469-7998.1992.tb07492.x

Billet, G., Hautier, L., de Muizon, C., and Valentin, X. (2011). Oldest cingulate skulls provide congruence between morphological and molecular scenarios of armadillo evolution. *Proc. R. Soc. Lond.* 1719, 2791–2797. doi: 10.1098/rspb.2010.2443

Billet, G., Hautier, L., and Lebrun, R. (2015). Morphological diversity of the bony labyrinth (inner ear) in extant xenarthrans and its relation to phylogeny. *J. Mammal.* 4, 658–672.

Bocherens, H., Cotte, M., Bonini, R. A., Straccia, P., Scian, D., Soibelzon, L., et al. (2017). Isotopic insight on paleodiet of extinct Pleistocene megafaunal Xenarthrans from Argentina. *Gondwana Res.* 48, 7–14. doi: 10.1016/j.gr.2017.04.003

Boscaini, A., Gaudin, T. J., Mamani Quispe, B., Münch, P., Antoine, P. O., and Pujos, F. (2019). New well-preserved craniodental remains of Simomylodon uccasamamensis (Xenarthra: Mylodontidae) from the Pliocene of the Bolivian Altiplano: phylogenetic, chronostratigraphic and palaeobiogeographical implications. *Zool. J. Linn. Soc.* 2, 459–486. doi: 10.1093/zoolinnean/zly075

Botton-Divet, L., Cornette, R., Houssaye, A., Fabre, A. C., and Herrel, A. (2017). Swimming and running: a study of the convergence in long bone morphology among semi-aquatic mustelids (Carnivora: Mustelidae). *Biol. J. Linn. Soc.* 121, 38–49. doi: 10.1093/biolinnean/blw027

Brakefield, P. M. (2006). Evo-devo and constraints on selection. *Trends Ecol. Evol.* 21, 362–368. doi: 10.1016/j.tree.2006.05.001

Castiglione, S., Serio, C., Tamagnini, D., Melchionna, M., Mondanaro, Di Febbraro, et al. (2019). A new, fast method to search for morphological convergence with shape data. *PLoS ONE* 14:226949. doi: 10.1371/journal.pone.0226949

Castiglione, S., Tesone, G., Piccolo, M., Melchionna, M., Mondanaro, A., Serio, C., et al. (2018). A new method for testing evolutionary rate variation and shifts in phenotypic evolution. *Methods Ecol. Evol.* 9, 974–983. doi: 10.1111/2041-210X.12954

Chiarello, A. G. (2008). "Sloth ecology. An overview of field studies," in *The Biology of the Xenarthra*, eds S. F. Vizcaíno, and W. J. Loughry (Gainesville: University Press of Florida), 269–280.

Cohen, B. L. (2018). Match and mismatch of morphological and molecular phylogenies: causes, implications, and new light on cladistics. *Zool. J. Linn. Soc.* 2, 516–527. doi: 10.1093/zoolinnean/zly004

De Iuliis, G., Bargo, M. S., and Vizcaíno, S. F. (2001). Variation in skull morphology and mastication in the fossil giant armadillos *Pampatherium* spp. and allied genera (Mammalia: Xenarthra: Pampatheriidae), with comments on their systematics and distribution. *J. Vertebr. Paleontol.* 4, 743–754.

de Oliveira, A. M., and Santos, C. M. D. (2018). Functional morphology and paleoecology of Pilosa (Xenarthra, Mammalia) based on a two-dimensional geometric Morphometrics study of the Humerus. *J. Morphol.* 279, 1455–1467. doi: 10.1002/jmor.20882

Delsuc, F., Kuch, M., Gibb, G. C., Karpinski, E., Hackenberger, D., Szpak, P., et al. (2019). Ancient mitogenomes reveal the evolutionary history and biogeography of sloths. *Curr. Biol.* 12, 2031–2042. doi: 10.1016/j.cub.2019.05.043

Delsuc, F., Vizcaíno, S. F., and Douzery, E. J. (2004). Influence of tertiary paleoenvironmental changes on the diversification of South American mammals: a relaxed molecular clock study within xenarthrans. *BMC Evol. Biol.* 1:11. doi: 10.1186/1471-2148-4-11

Egi, N. (2001). Body mass estimates in extinct mammals from limb bone dimensions: the case of North American hyaenodontids. *Palaeontology* 44, 497–528. doi: 10.1111/1475-4983.00189

Elton, S. (2002). A reappraisal of the locomotion and habitat preference of Theropithecus oswaldi. *Folia Primatol.* 73, 252–280. doi: 10.1159/000067457

Elton, S., Jansson, A. U., Meloro, C., Louys, J., Plummer, T., and Bishop, L. C. (2016). Exploring morphological generality in the Old World monkey postcranium using an ecomorphological framework. *J. Anat.* 228, 534–560. doi: 10.1111/joa.12428

Engelmann, G. F. (1985). "The phylogeny of the Xenarthra," in *The Evolution and Ecology of Armadillos, Sloths, and Vermilinguas*, ed. G. G. Montgomery (Washington, D.C: Smithsonian Institution Press), 51–64.

Falkingham, P. L. (2012). Acquisition of high resolution three-dimensional models using free, open-source, photogrammetric software. *Palaeontol. Electron.* 15, 1–15. doi: 10.26879/264

Fariña, R. A., and Vizcaíno, S. F. (1997). Allometry of the bones of living and extinct armadillos (*Xenarthra*, *Dasypoda*). *Zeitschrift für Saugetierkunde* 62, 65–70.

Fariña, R. A., Vizcaíno, S., and Storch, G. (2003). "Morphological studies in fossil and extant Xenarthra-(Mammalia)," in *Senckenbergiana Biologica, Band 83 Heft 1*, eds R. A. Fariña, S. Vizcaíno, and G. Storch (Stuttgart: Schweizerbart and Borntraeger science publishers).

Fau, M., Cornette, R., and Houssaye, A. (2016). Photogrammetry for 3D digitizing bones of mounted skeletons: potential and limits. *Cr. Palevol.* 15, 968–977. doi: 10.1016/j.crpv.2016.08.003

Felsenstein, J. (1985). Phylogenies and the comparative method. *Am. Nat.* 125, 1–15. doi: 10.1086/284325

Fernicola, J. C., Rinderknecht, A., Jones, W., Vizcaíno, S. F., and Porpino, K. (2017). A new species of neoglyptatelus (Mammalia, Xenarthra, Cingulata) from the Late Miocene of Uruguay provides new insights on the evolution of the dorsal armor in cingulates. *Ameghiniana* 3, 233–252. doi: 10.5710/AMGH.02.12.2017.3150

Figueirido, B., Pérez-Claros, J. A., Hunt, R. M., and Palmqvist, P. (2011). Body mass estimation in amphicyonid carnivoran mammals: a multiple regression approach from the skull and skeleton. *Acta Palaeontol. Pol.* 56, 225–247. doi: 10.4202/app.2010.0005

Finarelli, J. A., and Flynn, J. J. (2006). Ancestral state reconstruction of body size in the Caniformia (Carnivora, mammalia): the effects of incorporating data from the fossil record. *Syst. Biol.* 55, 301–313. doi: 10.1080/10635150500541698

Gaudin, T., and Wible, J. R. (2006). "The phylogeny of living and extinct armadillos (Mammalia, Xenarthra, Cingulata): a craniodental analysis," in *Amniote Paleobiology: Perspectives on the Evolution of Mammals, Birds, and Reptiles*, eds M. T. Carrano, T. Gaudin, R. W. Blob, and J. R. Wible (Chicago: University of Chicago Press), 153–198.

Giacomini, G., Scaravelli, D., Herrel, A., Veneziano, A., Russo, D., Brown, R. P., et al. (2019). 3D photogrammetry of bat skulls: perspectives for macro-evolutionary analyses. *Evol. Biol.* 46, 249–259. doi: 10.1007/s11692-019-09478-6

Gibb, G. C., Condamine, F. L., Kuch, M., Enk, J., Moraes-Barros, N., Superina, M., et al. (2016). Shotgun mitogenomics provides a reference phylogenetic framework and timescale for living xenarthrans. *Mol. Biol. Evol.* 33, 621–642. doi: 10.1093/molbev/msv250

Gingerich, P. D. (1990). Prediction of body mass in mammalian species from long bone lengths and diameters. *Contrib. Mus. Paleonotol. Univ. Mich.* 28, 79–92.

Goswami, A., Milne, N., and Wroe, S. (2011). Biting through constraints: cranial morphology, disparity and convergence across living and fossil carnivorous mammals. *Proc. R. Soc. B-Bio. Sci.* 1713, 1831–1839. doi: 10.1098/rspb.2010.2031

Gould, S. J. (1989). A developmental constraint in cerion, with comments of the definition and interpretation of constraint in evolution. *Evolution* 43:516. doi: 10.1111/j.1558-5646.1989.tb04249.x

Harmon, L. J., Kolbe, J. J., Cheverud, J. M., and Losos, J. B. (2005). Convergence and the multidimensional niche. *Evolution* 59, 409–421. doi: 10.1111/j.0014-3820.2005.tb00999.x

Herrera, C. M., Powell, J. E., Esteban, G. I., and del Papa, C. (2017). A new eocene dasypodid with caniniforms (Mammalia, Xenarthra, Cingulata) from northwest Argentina. *J. Mamm. Evol.* 3, 275–288. doi: 10.1007/s10914-016-9345-x

Hildebrand, M. (1985). "Digging of quadrupeds," in *Functional Vertebrate Morphology*, ed. M. Hildebrand (Cambridge: Cambridge University Press), 89–109.

Kley, N. J., and Kearney, M. (2007). "Adaptations for digging and burrowing," in *Fins into Limbs: Evolution*, ed. B. K. Hall (Chicago: University of Chicago Press), 284–309.

Klingenberg, C. P. (2016). Size, shape, and form: concepts of allometry in geometric morphometrics. *Dev. Genes Evol.* 226, 113–137. doi: 10.1007/s00427-016-0539-2

Losos, J. B. (2011). Convergence, adaptation, and constraint. *Evolution* 65, 1827–1840. doi: 10.1111/j.1558-5646.2011.01289.x

Mahler, D. L., Revell, L. J., Glor, R. E., and Losos, J. B. (2010). Ecological opportunity and the rate of morphological evolution in the diversification of greater Antillean Anoles. *Evolution* 64, 2731–2745. doi: 10.1111/j.1558-5646.2010.01026.x

Marshall, L. G., Butler, R. F., Drake, R. E., Curtis, G. H., and Tedford, R. H. (1979). Calibration of the great american interchange. *Science* 204, 272–279. doi: 10.1126/science.204.4390.272

Marshall, S. K. (2018). *Comparative Morphology of the Forelimb Digging Apparatus in Armadillos (Xenarthra: Cingulata, Dasypodidae)* Dissertation., Youngstown State University, Ohio.

Melchionna, M., Mondanaro, A., Serio, C., Castiglione, S., Di Febbraro, M., Rook, L., et al. (2020). Macroevolutionary trends of brain mass in Primates. *Biol. J. Linn. Soc.* 1, 14–25. doi: 10.1093/biolinnean/blz161

Meloro, C., Cáceres, N. C., Carotenuto, F., Sponchiado, J., Melo, G. L., Passaro, F., et al. (2015a). Chewing on the trees: constraints and adaptation in the evolution of the primate mandible. *Evolution* 69, 1690–1700. doi: 10.1111/evo.12694

Meloro, C., Clauss, M., and Raia, P. (2015b). Ecomorphology of carnivora challenges convergent evolution. *Org. Divers. Evol.* 15, 711–720. doi: 10.1007/s13127-015-0227-5

Meloro, C., Elton, S., Louys, J., Bishop, L. C., and Ditchfield, P. (2013). Cats in the forest: predicting habitat adaptations from humerus morphometry in extant and fossil Felidae (Carnivora). *Paleobiology* 39, 323–344. doi: 10.1666/12001

Meloro, C., and Raia, P. (2010). Cats and dogs down the tree: the tempo and mode of evolution in the lower carnassial of fossil and living carnivora. *Evol. Biol.* 37, 177–186. doi: 10.1007/s11692-010-9094-3

Meloro, C., Raia, P., Piras, P., Barbera, C., and O'Higgins, P. (2008). The shape of the mandibular corpus in large fissiped carnivores: allometry, function and phylogeny. *Zool. J Linn. Soc.* 154, 832–845. doi: 10.1111/j.1096-3642.2008.00429.x

Meloro, C., and Slater, G. J. (2012). Covariation in the skull modules of cats: the challenge of growing saber-like canines. *J. Vertebr. Paleontol.* 32, 677–685. doi: 10.1080/02724634.2012.649328

Mendel, F. C. (1985). Use of hands and feet of three-toed sloths (Bradypus variegatus) during climbing and terrestrial locomotion. *J. Mammal.* 66, 359–366. doi: 10.2307/1381249

Mielke, F., Amson, E., and Nyakatura, J. A. (2018). Morpho-functional analysis using procrustes superimposition by static reference. *Evol. Biol.* 4, 449–461. doi: 10.1007/s11692-018-9456-9

Milne, N., Toledo, N., and Vizcaíno, S. F. (2012). Allometric and group differences in the xenarthran femur. *J. Mamm. Evol.* 19, 199–208. doi: 10.1007/s10914-011-9171-0

Milne, N., Vizcaíno, S. F., and Fernicola, J. C. (2009). A 3D geometric morphometric analysis of digging ability in the extant and fossil cingulate humerus. *J. Zool.* 278, 48–56. doi: 10.1111/j.1469-7998.2008.00548.x

Monteiro, L. R., and Abe, A. S. (1999). Functional and historical determinants of shape in the scapula of xenarthran mammals: evolution of a complex morphological structure. *J. Morphol.* 241, 251–263. doi: 10.1002/(SICI)1097-4687(199909)241:3<251::AID-JMOR7>3.0.CO;2-7

Montgomery, G. G. (1985). "Impact of vermilinguas (Cyclopes, Tamandua: Xenarthra = Edentata) on arboreal ant populations," in *Ecology and Evolution of Sloths, Anteaters and Armadillos (Mammalia, Xenarthra = Edentata)*, ed. G. G. Montgomery (Washington, D.C: Smithsonian Institution Press), 351–363.

Nyakatura, J. A. (2011). The convergent evolution of suspensory posture and locomotion in tree sloths. *J. Mamm. Evol.* 19, 225–234. doi: 10.1007/s10914-011-9174-x

Nyakatura, J. A. (2012). The convergent evolution of suspensory posture and locomotion in tree sloths. *J. Mamm. Evol.* 3, 225–234. doi: 10.1007/s10914-011-9174-x

Nyakatura, J. A., and Fischer, M. S. (2011). Functional morphology of the muscular sling at the pectoral girdle in tree sloths: convergent morphological solutions to new functional demands? *J. Anat.* 219, 360–374. doi: 10.1111/j.1469-7580.2011.01394.x

Nyakatura, J. A., Petrovitch, A., and Fischer, M. S. (2010). Limb kinematics during locomotion in the twotoed sloth (Choloepus didactylus, Xenarthra) and its implications for the evolution of the sloth locomotor apparatus. *Zoology* 113, 221–234.

Piras, P., Sansalone, G., Teresi, L., Kotsakis, T., Colangelo, P., and Loy, A. (2012). Testing convergent and parallel adaptations in talpids humeral mechanical performance by means of geometric morphometrics and finite element analysis. *J. Morphol.* 273, 696–711. doi: 10.1002/jmor.20015

Polly, P. D. (2007). "Limbs in mammalian evolution," in *Fins into Limbs: Evolution*, ed. B. K. Hall (Chicago: University of Chicago Press), 245–268.

Presslee, S., Slater, G. J., Pujos, F., Forasiepi, A. M., Fischer, R., Molloy, K., et al. (2019). Palaeoproteomics resolves sloth relationships. *Nat. Ecol. Evol.* 3, 1121–1130. doi: 10.1038/s41559-019-0909-z

Prothero, D. R. (2016). *The Princeton Field Guide to Prehistoric Mammals*, Vol. 112. Princeton, NJ: Princeton University Press.

Pujos, F., Gaudin, T. J., De Iuliis, G., and Cartelle, C. (2012). Recent advances on variability, morpho-functional adaptations, dental terminology, and evolution of sloths. *J. Mamm. Evol.* 19, 159–169. doi: 10.1007/s10914-012-9189-y

Raia, P., Carotenuto, F., Meloro, C., Piras, P., and Pushkina, D. (2010). The shape of contention: adaptation, history, and contingency in ungulate mandibles. *Evolution* 64, 1489–1503. doi: 10.1111/j.1558-5646.2009.00921.x

Raia, P., Carotenuto, F., Passaro, F., Piras, P., Fulgione, D., Werdelin, L., et al. (2013). Rapid action in the palaeogene, the relationship between phenotypic and taxonomic diversification in Coenozoic mammals. *Proc. Biol. Sci.* 280, 20122244–20122244. doi: 10.1098/rspb.2012.2244

Raia, P., Castiglione, S., Serio, C., Mondanaro, A., Melchionna, M., Di Febbraro, M., et al. (2020). *RRphylo: Phylogenetic Ridge Regression Methods for Comparative Studies. R package version* 2.4.4. Available online at: https://rdrr.io/cran/RRphylo/ (accessed September 3, 2019).

Rohlf, F. J., and Slice, D. (1990). Extensions of the procrustes method for the optimal superimposition of landmarks. *Syst. Biol.* 39, 40–59. doi: 10.2307/2992207

Sansalone, G., Castiglione, S., Raia, P., Archer, M., Dickson, B., Hand, S., et al. (2020). Decoupling functional and morphological convergence, the study case of fossorial mammalia. *Front. Earth Sci.* 8:112. doi: 10.3389/feart.2020.00112

Sansalone, G., Colangelo, P., Loy, A., Raia, P., Wroe, S., and Piras, P. (2019). Impact of transition to a subterranean lifestyle on morphological disparity and integration in talpid moles (Mammalia, Talpidae). *BMC Evol. Biol.* 19:179. doi: 10.1186/s12862-019-1506-0

Serio, C., Castiglione, S., Tesone, G., Piccolo, M., Melchionna, M., Mondanaro, A., et al. (2019). Macroevolution of toothed whales exceptional relative brain size. *Evol. Biol.* 4, 332–342. doi: 10.1007/s11692-019-09485-7

Shingleton, A. W., Frankino, W. A., Flatt, T., Nijhout, H. F., and Emlen, D. J. (2007). Size and shape: the developmental regulation of static allometry in insects. *BioEssays* 29, 536–548. doi: 10.1002/bies.20584

Simpson, G. G. (1980). *Splendid Isolation: The Curious History of South American Mammals*, Vol. 275. New Haven: Yale University Press.

Smaers, J. B., Mongle, C. S., and Kandler, A. (2016). A multiple variance Brownian motion framework for estimating variable rates and inferring ancestral states. *Biol. J. Linn. Soc.* 118, 78–94. doi: 10.1111/bij.12765

Speed, M. P., and Arbuckle, K. (2016). Quantification provides a conceptual basis for convergent evolution. *Biol. Rev.* 92, 815–829. doi: 10.1111/brv.12257

Springer, M. S., Murphy, W. J., Eizirik, E., and O'Brien, S. J. (2003). Placental mammal diversification and the Cretaceous-Tertiary boundary. *Proc. Natl. Acad. Sci. U.S.A.* 100, 1056–1061. doi: 10.1073/pnas.0334222100

Toledo, N., Bargo, M. S., Cassini, G. H., and Vizcaíno, S. F. (2012). The forelimb of early miocene sloths (Mammalia, Xenarthra, Folivora): morphometrics and functional implications for substrate preferences. *J. Mamm. Evol.* 19, 185–198. doi: 10.1007/s10914-012-9185-2

Toledo, N., Bargo, M. S., and Vizcaíno, S. F. (2015). Muscular reconstruction and functional morphology of the hind limb of santacrucian (Early Miocene) sloths (Xenarthra, Folivora) of Patagonia. *Anat. Rec.* 5, 842–864. doi: 10.1002/ar.23114

Toledo, N., Bargo, M. S., Vizcaíno, S. F., De Iuliis, G., and Pujos, F. (2017). Evolution of body size in anteaters and sloths (Xenarthra, Pilosa): phylogeny, metabolism, diet and substrate preferences. *Earth Environ. Sci. Trans R. Soc. Edinb.* 106, 289–301. doi: 10.1017/S1755691016000177

Varela, L., Tambusso, P. S., McDonald, H. G., and Fariña, R. A. (2019). Phylogeny, macroevolutionary trends and historical biogeography of sloths: insights from a Bayesian morphological clock analysis. *Syst. Biol.* 2, 204–218. doi: 10.1093/sysbio/syy058

Vizcaíno, S. F., Bargo, M. S., and Cassini, G. H. (2006). Dental occlusal surface area in relation to body mass, food habits and other biological features in fossil xenarthrans. *Ameghiniana* 1, 11–26.

Vizcaíno, S. F., Bargo, M. S., and Fariña, R. A. (2008). "Form, function, and paleobiology in xenarthrans," in *The Biology of the Xenarthra*, eds S. F. Vizcaíno, and W. J. WJ Loughry (Gainesville: University Press of Florida), 86–99.

Vizcaíno, S. F., and Bargo, S. M. (2003). Limb reconstruction of Eutatus seguini(Mammalia: Xenarthra: Dasypodidae), Paleobiological implications. *Ameghiniana* 40, 89–101.

Vizcaíno, S. F., Blanco, R. E., Bender, J. B., and Milne, N. (2010). Proportions and function of the limbs of glyptodonts (Mammalia, Xenarthra). *Lethaia* 44, 93–101. doi: 10.1111/j.1502-3931.2010.00228.x

Vizcaíno, S. F., De Iuliis, G., and Bargo, M. S. (1998). Skull shape, masticatory apparatus, and diet of Vassallia and Holmesina (Mammalia: Xenarthra: Pampatheriidae): when anatomy constrains destiny. *J. Mamm. Evol.* 4, 291–322. doi: 10.1023/A:1020500127041

Vizcaíno, S. F., Farina, R. A., and Mazzetta, G. V. (1999). Ulnar dimensions and fossoriality in armadillos. *Acta Theriol.* 44, 309–320.

Vizcaíno, S. F., and Milne, N. (2002). Structure and function in armadillo limbs (Mammalia: Xenarthra: Dasypodidae). *J. Zool.* 1, 117–127. doi: 10.1017/S0952836902000717

Vizcaíno, S. F., Zárate, M., Bargo, M. S., and Dondas, A. (2001). Pleistocene burrows in the Mar del Plata area [Argentina] and their probable builders. *Acta Palaeontol Pol.* 46, 289–301.

Voje, K. L., Hansen, T. F., Egset, C. K., Bolstad, G. H., and Pélabon, C. (2014). Allometric constraints and the evolution of allometry. *Evolution* 68, 866–885. doi: 10.1111/evo.12312

Walmsley, A., Elton, S., Louys, J., Bishop, L. C., and Meloro, C. (2012). Humeral epiphyseal shape in the Felidae: the influence of phylogeny, allometry, and locomotion. *J. Morphol.* 273, 1424–1438. doi: 10.1002/jmor.20084

Webb, S. D. (2006). The great american biotic interchange: patterns and processes1. *Ann. Missouri Bot. Gard.* 93, 245–257.

White, J. L. (2010). Indicators of locomotor habits in xenarthrans: evidence for locomotor heterogeneity among fossil sloths. *J. Vertebr. Paleontol.* 13, 230–242. doi: 10.1080/02724634.1993.10011502

Wroe, S., and Milne, N. (2007). Convergence and remarkably consistent constraint in the evolution of carnivore skull shape. *Evolution* 5, 1251–1260. doi: 10.1111/j.1558-5646.2007.00101.x

Zelditch, M. L., Swiderski, D. L., and Sheets, H. D. (2012). *Geometric Morphometrics for Biologists*. Cambridge, MA: Academic Press.

Conflict of Interest: The authors declare that the research was conducted in the absence of any commercial or financial relationships that could be construed as a potential conflict of interest.